Neutron scattering study of the magnetic excitations in metallic and superconducting $La_{2-x}Sr_xCuO_{4-y}$

T. R. Thurston,* R. J. Birgeneau,* M. A. Kastner, and N. W. Preyer
Department of Physics, Massachusetts Institute of Technology, Cambridge, Massachusetts 02139

G. Shirane and Y. Fujii†
Physics Department, Brookhaven National Laboratory, Upton, New York 11973-6000

K. Yamada,* Y. Endoh,* K. Kakurai, and M. Matsuda
Department of Physics, Tohoku University, Sendai 980, Japan

Y. Hidaka and T. Murakami
NTT Opto-Electronics Laboratories, Nippon Telegraph and Telephone Corporation, Tokai, Ibaraki 319-11, Japan

(Received 22 March 1989)

We report on neutron scattering studies of the dynamic spin correlations in $La_{2-x}Sr_xCuO_{4-y}$. Two superconducting and one nonsuperconducting single crystals were studied. All three of the samples exhibited metallic normal-state resistivity modified by corrections consistent with localization effects. The structure factor $S(\mathbf{Q},\omega)$ measured in these samples reflects to a first approximation short-range two-dimensional antiferromagnetic spin correlations closely related to those found in insulating La_2CuO_4. In addition, $S(\mathbf{Q},\omega)$ measured in the superconducting samples has an incommensurate, double-peaked structure which is not present in the nonsuperconducting crystal. The integrated ($\int dQ$) intensities of the scattering at both concentrations are nearly independent of temperature over the range $k_BT \gg \hbar\omega$ to $k_BT \ll \hbar\omega$ for energy transfers greater than ~ 6 meV. Furthermore, the difference in the temperature dependence of the intensity between the nonsuperconducting and superconducting samples for energy transfers less than ~ 6 meV suggests that a gap may be forming in the magnetic excitation spectrum of the superconducting samples. The relationship of these results to the superconductivity in $La_{2-x}Sr_xCuO_{4-y}$ is discussed.

I. INTRODUCTION

A variety of experiments has shown interesting microscopic magnetic effects in $La_{2-x}Sr_xCuO_{4-y}$.[1-10] In lightly doped La_2CuO_{4-y}, neutron scattering experiments[1] have shown that the spin system undergoes a transition into a three-dimensional (3D) Néel state, and that pronounced two-dimensional spin fluctuations[2] with a very large energy scale exist at temperatures above the Néel transition. Muon-spin resonance (μSR) (Ref. 3) and light scattering experiments[4] have also probed the antiferromagnetic behavior found in lightly doped La_2CuO_{4-y}. In more heavily doped $La_{2-x}Sr_xCuO_{4-y}$, neutron scattering experiments[5] have shown that doping beyond $x \simeq 0.02$ destroys long-range order. These same neutron scattering measurements demonstrated that short-range magnetic order exists in heavily doped samples, corroborating earlier reports[6] which indicated that magnetic moments persist in $La_{2-x}Sr_xCuO_{4-y}$. The magnetism of $La_{2-x}Sr_xCuO_{4-y}$ has also been probed in nuclear magnetic resonance (NMR) (Ref. 7) and μSR (Ref. 8) experiments; these measurements show that some type of local spin ordering takes place at low temperatures, even in $x \sim 0.15$ superconducting samples. Finally, the nature of the spin correlations in superconducting samples has been probed in double-axis (energy integrating) neutron scattering measurements,[9,10] which have indicated the presence of an elaborate incommensurate structure in $S(\mathbf{Q},\omega)$.

In this article we extend previous neutron scattering work to explore directly the spin dynamics in $La_{2-x}Sr_xCuO_{4-y}$. The experiments described in this paper are inelastic neutron scattering studies on one nonsuperconducting ($x \sim 0.06$) and two superconducting ($x \sim 0.11$) samples. The samples, all of which were grown at Nippon Telegraph and Telephone Laboratories (NTT), are crystallographically of high quality; consequently, we have been able to make rather detailed studies of the dynamic spin correlations. We report a number of new results. Principal among them is that the incommensurate structure appears to be present only in superconducting samples. The energy dependence of the scattering has also been mapped out using inelastic neutron scattering (triple-axis) techniques, and the intensity of the inelastic scattering at energy transfers greater than ~ 6 meV measured in both the nonsuperconducting and the superconducting samples turns out to be nearly independent of temperature from 5 to 300 K. Further, the difference in the temperature dependence of the intensity between the nonsuperconducting and superconducting samples for en-

ergy transfers less than ~6 meV suggests that a gap is forming in the magnetic excitation spectrum of the superconducting samples.

The format of this paper is as follows: In Sec. II the crystal structure and growth are described. A brief review of the relevant neutron scattering cross sections is presented in Sec. III, and sample characterization measurements are presented in Sec. IV. Neutron scattering experimental results are presented in Sec. V. Finally, in Sec. VI we discuss the results and their relationship to current theories of the superconducting state.

II. PRELIMINARY DETAILS

The crystalline and magnetic structures of La_2CuO_4 are shown in Fig. 1(a). The open arrows indicate the direction of rotation of the CuO_6 octahedra at the tetragonal-to-orthorhombic structural phase transition, while the closed arrows indicate copper spin directions in the 3D Néel state of undoped La_2CuO_4. In the low-temperature phase the structure is orthorhombic, space group *Cmca*, with lattice constants $b \gg c > a$. We shall use *Cmca* notation exclusively in this paper. In Fig. 1(b) we show the orthorhombic reciprocal lattice; almost all of the results presented here were taken along the $(1,k,0)$ and $(0,k,1)$ magnetic 2D rods.

Single-crystal samples were grown at NTT using a CuO flux method. We discuss briefly the growth technique here; full details are given by Hidaka *et al.*[11] High-quality La_2O_3 (99.9% purity), $SrCO_3$ (99.9% purity), and CuO (99.9% purity) powder were used as the starting materials for crystal growth. The CuO flux ratio used for the single-crystal growth was about 80%; this is slightly below the value of the eutectic point of the $(La,Sr)_2CuO_4$-CuO system. The mixture was loaded into a platinum crucible, heated up to 1300 °C in air, and then slow cooled at the rate of 2–4 °C per hour. Nucleation of the crystals began around 1100 °C, although the explicit value depended on the Sr concentration. This technique produced large single crystals for Sr concentrations in the melt (x_m) up to 0.5; however, the actual amount of Sr incorporated into the single crystals (x) was much less. The final concentration in the crystal x varied from 0.016 to 0.15 as the concentration in the melt, x_m, varied from 0.02 to 0.5.

III. MAGNETIC NEUTRON SCATTERING CROSS SECTIONS

In this section we review briefly the magnetic neutron scattering technique; for a full discussion see Ref. 12. A scattering event is considered in which monochromatized neutrons with energy E_i and momentum $\mathbf{k}_i$ are scattered off the sample into a state with energy E_f and momentum $\mathbf{k}_f$. Each scattering event is distinguished by two quantities, the momentum transferred to the sample, $\mathbf{Q}=\mathbf{k}_i-\mathbf{k}_f$, and the energy transferred to the sample, $\hbar\omega=E_i-E_f$. The cross section for spin only scattering is then[12]

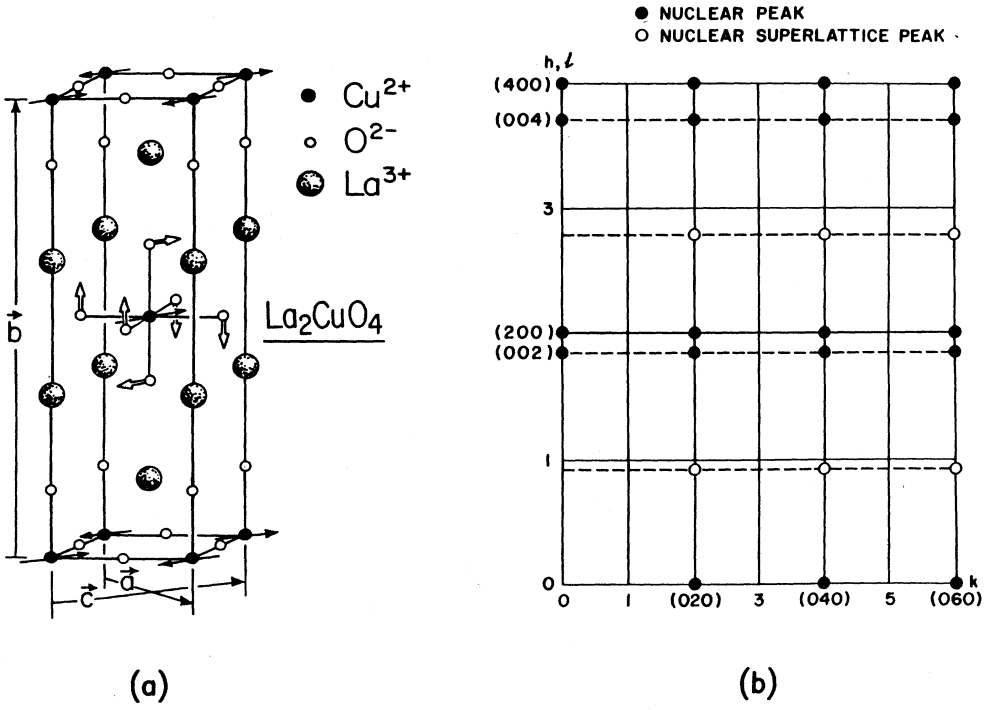

FIG. 1. (a) Crystal structure of La_2CuO_4. The center arrows show the motion of oxygen atoms at the tetragonal-to-orthorhombic structure phase transition and the black arrows denote spin directions in the 3D Néel state of the undoped material. (b) Reciprocal lattice; most of the data presented here were taken on the $(1,k,0)$ and $(0,k,1)$ rods.

$$\frac{\partial^2\sigma}{\partial\Omega_f\,\partial E_f}\sim|f(\mathbf{Q})|^2\frac{|\mathbf{k}_f|}{|\mathbf{k}_i|}\sum_\alpha(1-\hat{Q}_\alpha^2)S^{\alpha\alpha}(\mathbf{Q},\omega)\ , \tag{1a}$$

where

$$S^{\alpha\alpha}(\mathbf{Q},\omega)=\frac{1}{2\pi}\int_{-\infty}^{+\infty}dt\,e^{i\omega t}\sum_{\mathbf{R}}e^{i\mathbf{Q}\cdot\mathbf{R}}\langle S_0^\alpha(0)S_{\mathbf{R}}^\alpha(t)\rangle\ . \tag{1b}$$

Here $f(\mathbf{Q})$ is the magnetic form factor for the spins, and α refers to the x, y, or z axes. The quantity $S^{\alpha\alpha}(\mathbf{Q},\omega)$, known as the van Hove scattering function or structure function, is the Fourier transform in both space and time of the spin-spin correlation function $\langle S_0^\alpha(0)S_{\mathbf{R}}^\alpha(t)\rangle$. This quantity is a thermal average over the correlations between the components along the αth axis of a spin at the origin 0 at time zero and a spin at site $\mathbf{R}$ at time t.

Instrumental resolution effects are always present in neutron scattering experiments, and they must be considered when interpreting data. Indeed, in some situations the geometry of the instrumental resolution may be matched to the geometry of the scattering to enhance the measured signal relative to the background. The resolution appropriate for triple-axis scans may be modeled quite well by a four-dimensional ellipsoid in momentum-energy space.[13] As an example, we consider the case where the spectrometer is set with 13.7 meV incident neutrons at zero-energy transfer and momentum transfer $2\pi/a=1.17$ Å^{-1}. The projection of the resolution function on the energy-transfer axis is then 1 meV full width at half maximum (FWHM), and the projection of the resolution function on the scattering plane is an ellipsoid which has a principal axis approximately along $\mathbf{Q}$. The width longitudinal to $\mathbf{Q}$ of this projection is of order $\sim$0.02 Å^{-1} FWHM, and the width transverse to $\mathbf{Q}$ is of order $\sim$0.1 Å^{-1} FWHM. In the third direction in momentum-transfer space the resolution ellipsoid has a projection of $\sim$0.1 Å^{-1} FWHM; the spectrometer cannot be scanned along this third direction, however. We emphasize that the above numbers are projections of the resolution ellipsoid onto the axes; the resolution ellipsoid itself can, in general, have any orientation in $(\hbar\omega)$-$\mathbf{Q}$ space. The elongated nature of the resolution function projection onto the scattering plane suggests that the signal and more importantly the signal-to-noise ratio may be enhanced if the long axis of the projection ellipsoid is oriented parallel to the 2D rod of magnetic scattering. In fact, the optimum focusing position also depends on the geometry of $S(\mathbf{Q},\omega)$, so this condition is not satisfied exactly. To exploit instrumental focusing, the k position along the 2D magnetic rod at which one does a scan must be varied as the energy is changed so that the resolution ellipsoid is always in the focusing position. In practice, the position along the rod at which focusing occurs has been determined experimentally; however, simulations in which the instrumental resolution function is accounted for predict reasonably well the experimentally determined focusing position.

IV. SAMPLE CHARACTERIZATION MEASUREMENTS

In order to characterize our samples, a variety of fundamental quantities have been measured. These include measurements of the tetragonal-to-orthorhombic structural transition temperature T_0, the μSR spin freezing temperature T_f,[8] the room-temperature lattice constants, and the superconducting transition temperature. All of these quantities along with the labels assigned to these crystals in previous work[5,10] are listed in Table I.

The resistivities of NTT-10 and NTT-30 are shown in Fig. 2. Because of the irregular shapes of these crystals, the magnitude of the resistivity is uncertain in each case to within a factor of $\sim$2. The resistivity perpendicular to the CuO_2 planes in NTT-30 is about 100 times larger than that in the planes. Such large anisotropy is typical of the highest-quality single crystals, as discussed, for example, by Preyer *et al.*[14] In the following, we restrict our discussion to the lower, in-plane resistivity.

For both samples the normal-state resistivity shows behavior intermediate between that of pure single crystals of La_2CuO_{4+y} and that of ceramics with superconducting transition temperatures of $\sim$40 K. The former show thermally activated conductivity, albeit with an activation energy that is temperature dependent in a way consistent with phonon-assisted hopping.[15] The latter have metallic resistivity, increasing linearly with T, above T_c. The two crystals measured here display resistivity that increases at low T, but only by a factor $\lesssim$4 between 250 and 5 K, even for the more resistive of the two. This is to be compared with the resistivity of as-prepared La_2CuO_{4+y}, for which the resistivity increases from 10 to 10^6 Ω cm in the same temperature range.[15]

The temperature dependence of the normal-state resistivity for NTT-30 is consistent with that predicted by the theory of weak localization in two dimensions.[16] The latter predicts a decrease in conductance at low temperatures proportional to $\ln(T)$ with a prefactor that is of order $e^2/\pi h$ and is independent of the conductance itself. We find that the increase of resistivity for NTT-30 can be

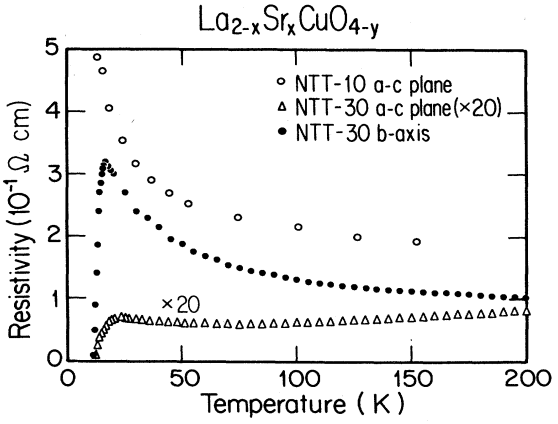

FIG. 2. Resistivity of NTT-10 and NTT-30. The in-plane resistivity of NTT-30 has been scaled by a factor of 20.

TABLE I. T_f for NTT-30 and NTT-35 was measured in a sample grown under identical conditions to these samples. The lattice constants were measured at 300 K.

		Sample properties						
Label	x	Vol. (cc)	a (Å)	b (Å)	c (Å)	T_0 (K)	T_c (K)	T_f (K)
NTT-2	0	0.40	5.36	13.15	5.41	503		
NTT-10	0.06	0.45	5.36	13.18	5.39	428		6
NTT-30	0.11	0.75	5.36	13.22	5.36	265	10	~5
NTT-35	0.11	1.45	5.36	13.22	5.36	265	10	~5

fit adequately with the $\ln(T)$ form, and that the prefactor is within a factor of ~4 of $e^2/\pi h$. The increase in resistivity of NTT-10 can also be adequately fit with a $\ln(T)$ form, but for this sample the prefactor disagrees with the weak-localization prediction, $e^2/\pi h$, by a factor of ~50. Weak-localization theory is valid only when the change in conductance due to localization effects ΔG is much smaller than the conductance itself. In NTT-10 $\Delta G/G > 1$, while in NTT-30 $\Delta G/G \sim 0.15$. Moreover, the magnitude of the resistivity of NTT-10 measured here is considerably larger than that of other samples with comparable strontium concentrations,[17] and the crystal has an irregular geometry, so it is difficult to make quantitative statements about the resistivity of this sample. It is therefore reasonable that NTT-30 exhibits a conductance which is consistent with 2D weak-localization theory while NTT-10 exhibits a conductance which is not. Dedicated experiments to test the predictions of the weak localization theory are underway. Based on experience with other 2D systems, it appears that the nonsuperconducting crystal displays localization behavior on a shorter length scale than the superconducting ones. In other words, superconductivity occurs only when disorder-induced backscattering is sufficiently weak.

Magnetization measurements were taken on a piece of dimensions $6\times6\times2$ mm^3 broken off from the superconducting sample, NTT-35. The experiments were done in both the field-cooled (FC) and zero-field-cooled (ZFC) configurations. From these measurements we calculated that the susceptibility was ~80% of $-1/4\pi$ in external fields less than 10 G. The character of the superconducting transition may be judged from the data shown in Fig. 3, which exhibits magnetization versus temperature taken in the ZFC configuration. The magnetization measured in NTT-35 is denoted by the open circles, while the solid circles represent the behavior observed in a sample identical to NTT-35 which had been annealed in an oxygen atmosphere. Apparently, an oxygen concentration inhomogeneity has produced a variation of T_c of ~5 K in different regions of our samples. This spread in T_c is consistent with the rounding we observed in the tetragonal-orthorhombic structural phase transition. We remark that all neutron scattering experiments reported herein were performed on samples in their as-grown state.

The 2D antiferromagnetic correlation length, ξ_{2D}, has been measured in previous double-axis (energy integrating) experiments on a number of doped samples, including those examined in this paper.[5,10] It was found that ξ_{2D} is approximately independent of temperature, but that the correlation length does depend on the strontium concentration. Figure 4 shows the 2D correlation length versus strontium concentration, x. The line is the average separation between the holes introduced by strontium doping; experimentally the 2D antiferromagnetic correlation length is of the order of the hole separation. In all three of the samples studied here, $\xi_{2D}=18\pm6$ Å. The large error in this measurement comes from uncertainties in the line shape of the scattering.

Two properties which reflect the bulk characteristics of a sample, the μSR-spin-freezing temperature T_f,[8] and the structural-phase-transition temperature T_0, have also been measured. The spin-freezing temperatures of NTT-10 and a sample grown under identical conditions to NTT-30 and NTT-35 were determined by Uemura and co-workers.[18] They found that the spin-freezing transition occurs at 6 K in NTT-10 and at ~5 K in the sample grown under identical conditions to NTT-30 and NTT-35. T_0 was measured by monitoring the temperature dependence of an orthorhombic-phase superlattice peak, typically the (0,2,1). The strontium and oxygen homogeneity of the samples may be estimated from the amount of rounding in T_0, which we found to be less than 25 K for all three samples. Using this value and previous results[5,19] we calculated the spreads in x and y in $La_{2-x}Sr_xCuO_{4-y}$ to be less than 0.012. From Fig. 3 of Ref. 5, as well as from chemical analysis, we estimate $x=0.06\pm0.02$ for NTT-10 and $x=0.11\pm0.02$ for NTT-

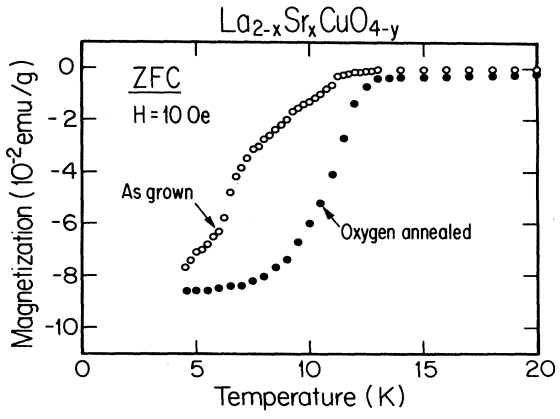

FIG. 3. Magnetization measurements taken in the ZFC configuration at a field of 10 Oe. The as-grown data are from measurements on a piece of NTT-35 and the oxygen annealed data are from measurements on a sample grown under identical conditions to NTT-35.

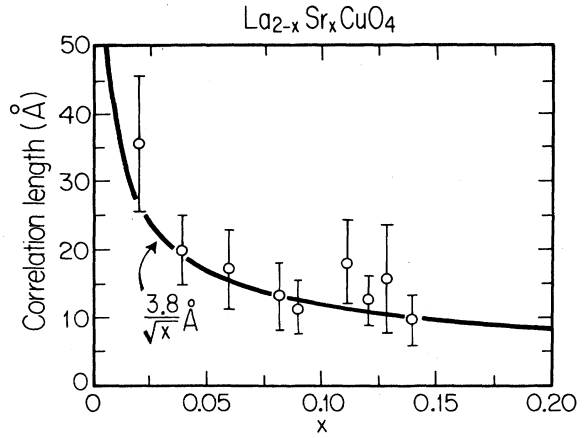

FIG. 4. Magnetic correlation length vs strontium concentration, x. The line represents the average separation between holes introduced by Sr^{2+} doping.

30 and NTT-35. We emphasize that measurements of T_0 reflect bulk properties of the material. Therefore, our samples have very uniform oxygen and strontium concentrations; consequently, the superconductivity must be a bulk rather than surface effect, consistent with our flux expulsion measurements.

We now discuss our overall conclusions about the character of our samples. Assuming that the properties of this system depend solely on hole content, and using Fig. 4 of Weidinger *et al.*,[8] the spin-freezing and transport properties indicate that NTT-10 is just barely nonsuperconducting with a net hole concentration $p \sim 0.05$ and that NTT-30 and NTT-35 are just barely superconducting with $p \sim 0.07$. Using the data found in Johnston *et al.*,[19] Torrance *et al.*,[20] and Birgeneau *et al.*,[5] the lattice constants and structural-phase-transition temperature values are consistent with the spin-freezing and transport characterization of the samples, if it is assumed that all three samples are oxygen deficient. We show in Fig. 5 the position of samples studied here and in some of our other work[2,21] on a schematic temperature versus hole concentration phase diagram. The data in this paper will show that samples which are just barely nonsuperconducting and just barely superconducting exhibit dramatically different microscopic magnetic behavior.

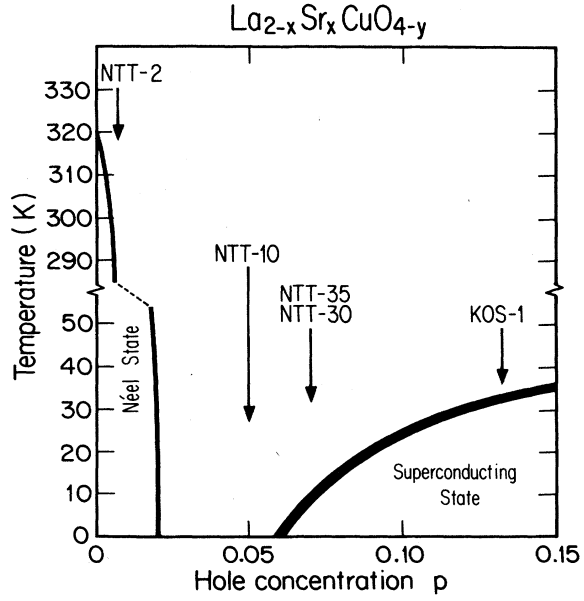

FIG. 5. Hole concentration vs temperature phase diagram showing the character of several samples studied at Brookhaven National Laboratory.

V. NEUTRON SCATTERING MEASUREMENTS

In this section we describe the results of our neutron scattering experiments. The measurements were done on spectrometers H7 and H4M at the Brookhaven National Laboratory High Flux Beam Reactor; a variety of experimental configurations was used in order to optimize the visibility of the magnetic scattering above the background. Data were taken with either the incident or final neutron energy fixed (E_i- or E_f-fixed mode) at one of 13.7, 14.7, or 30.5 meV, while neutrons with subharmonic wavelengths were removed with pyrolitic graphite filters.

The scattering observed in one of the superconducting samples, NTT-35, is shown in Figs. 6–9. We note that experiments on NTT-30 gave results entirely consistent with experiments on NTT-35. The scattering observed at 300 K at various energy transfers is shown in Fig. 6. Two series of scans showing the temperature dependence of the 6 and 4.5 meV response functions are given in Figs. 7 and 8, while in Fig. 9 two scans taken at 5 K with different energy transfers are presented. In Fig. 6 the scans were taken in the E_i-fixed configuration; the intensity must therefore be multiplied by a correction factor,[22] $\tan(\theta_A)/k_f^3$, where θ_A is the analyzer scattering angle. Thus the scans at higher absolute energy transfers in Fig. 6 have corrections which considerably reduce the experimentally measured intensity in obtaining the intrinsic $S(\mathbf{Q},\omega)$. These corrections have not been applied to the data shown in Fig. 6. The data in Figs. 7–9 were taken in the E_f-fixed mode; consequently, no significant intensity corrections are needed for these data.

A number of very interesting features may be seen in the data of Figs. 6–9. First, $S(\mathbf{Q},\omega)$ in the superconducting sample exhibits peaks which are split off from the (1,0,0) antiferromagnetic peak position. At 300 K this incommensurability is clearly visible at 9 and 15 meV; as is evident in Figs. 7–9, at lower temperatures $S(\mathbf{Q},\omega)$ at 6, 4.5, and 1.5 meV also exhibits the same incommensurability. This incommensurability has been observed previously in energy integrating $[\int S(\mathbf{Q},\omega)d\omega]$ double-axis scans.[9,10] We remark that the incommensurability observed in the present results is not clearly resolved at all energies, temperatures and experimental configurations; we believe that this occurs at least partly because the temperature-dependent inelastic background and instru-

mental resolution effects can easily obscure the intrinsic signal. The fact that the double-peak structure becomes more clearly resolved at lower temperatures nonetheless appears to be intrinsic; however, we caution that it is difficult to make quantitative statements.

The incommensurability appears to increase slightly between the energies of 1.5 and 9 meV, and then at larger energies appears to decrease again. This can be seen in the data presented in Fig. 6, where the 15 meV scan exhibits a smaller incommensurability than the 9 meV scan. We remark that other data not shown here support this decrease in incommensurability at large energy transfers; however, more experimental work is necessary to document convincingly this novel behavior.

It is impossible to determine the intrinsic signal in the zero-energy transfer scan of Fig. 6 because the elastic background from parasitic scattering events is too large.

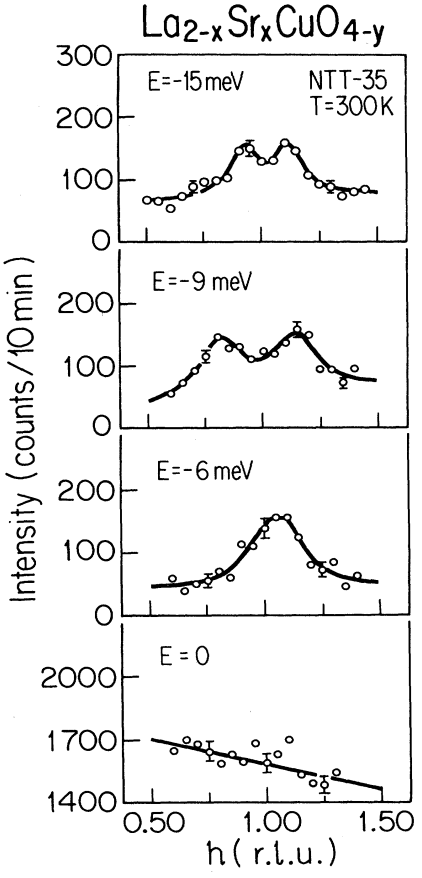

FIG. 6. Constant-E scans across the 2D magnetic rod in NTT-35. The spectrometer was set in the E_i-fixed mode at 13.7 meV and the collimation was 40′-40′-40′-80′. Since these data were taken in the E_i-fixed mode, the relative intensity at various energy transfers must be scaled by the $\tan(\theta_A)/k_f^3$ correction factor described in the text. The focusing positions along the 2D magnetic rod for scans with $E=-1.5$, -3.0, -6.0, -9.0, and -15 meV were $k=0.90$, 1.15, 1.70, 2.15, and 3.0 r.l.u., respectively.

This result apparently contradicts a previous measurement,[10] where a rather large elastic signal which exhibited the symmetry in momentum-transfer space characteristic of an intrinsic signal was observed. The difference between the data presented here and that presented in earlier work is that the energy of the incident neutron was 13.7 meV for the data shown in Fig. 6, while it was 14.7 meV in the previous measurement. We conclude that most of the zero-energy transfer signal measured previously is not intrinsic, although more detailed measurements will be needed to document this convincingly. A mystery which remains to be solved is how a nonintrinsic scattering process can have the symmetry of the reciprocal lattice.

Because the crystal was mounted in an [001] zone, the measurements described above only determine the incommensurability along (1,0,0) and (0,0,1). We have carried out some preliminary measurements in the [010] zone in an attempt to map out the full 2D geometry of $S(\mathbf{Q},\omega)$. However, in the [010] zone the background increases by a factor of ~ 3; consequently we were unable to obtain convincing data in a reasonable length of time. The issue of the full 2D geometry will be addressed in future experiments.

In Figs. 10 and 11, we show data taken on the nonsuperconducting sample, NTT-10. The scans in Fig. 10 were taken with configurations identical to those used to

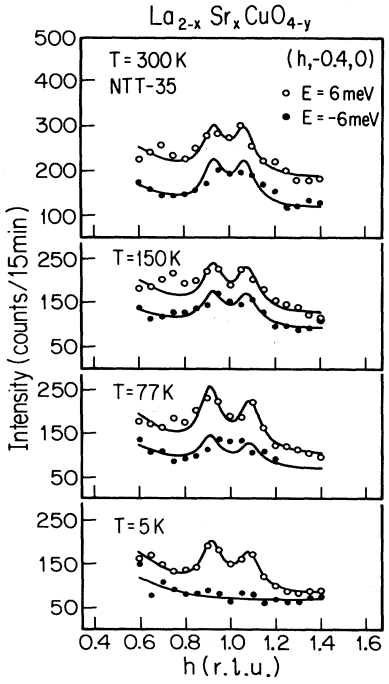

FIG. 7. Temperature dependence of the $+6$ and -6 meV scattering in NTT-35. The spectrometer was set in the E_f-fixed mode at 30.5 meV and the collimation was 40′-40′-40′-80′. The line through the -6 meV scattering is from a fit to the $+6$ meV scattering scaled by the detailed balance factor as discussed in the text.

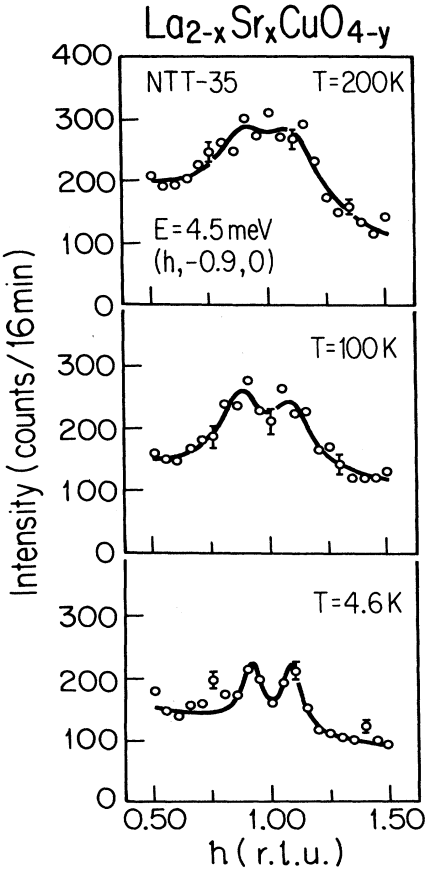

FIG. 8. Temperature dependence of the 4.5 meV scattering in NTT-35. The spectrometer was set in the E_f-fixed mode at 30.5 meV and the collimation was 40′-40′-40′-80′.

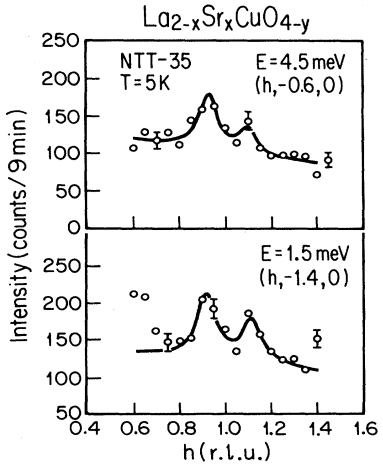

FIG. 9. 1.5 and 4.5 meV scans taken at 5 K in NTT-35. The spectrometer was set in the E_f-fixed mode at 13.7 meV and the collimation was 40′-80′-40′-80′.

obtain the data shown in Fig. 6, while the scans in Fig. 11 were taken with conditions comparable to those used in obtaining the data shown in Fig. 9. We note that a small correction[23] must be applied to obtain intrinsic relative intensities of the scans shown in Fig. 11; this correction decreases the intensity of the 9 meV scans relative to the 3 meV scans by 20%.

It is clear from the data in Figs. 10 and 11 that there is no evidence for incommensurability at any energy transfer at any temperature in this nonsuperconducting sample, since all peaks are symmetric and centered about $h=1$; similar results were reported in Ref. 5. Fits to a double-peaked scattering function indicate that any possible incommensurability which may have been obscured by disorder and instrumental resolution effects is less than 0.03 Å^{-1}. As can be seen in Fig. 10, the line shape at 300 K does not change in width between 3 and 15 meV, and indeed this width is just that determined in Ref. 5 from double-axis energy-integrating measurements on NTT-10. Further, the line shape of the 3 and 9 meV scattering shown in Fig. 11 is approximately independent of temperature. The dramatic difference in the microscopic magnetic behavior observed in nonsuperconduct-

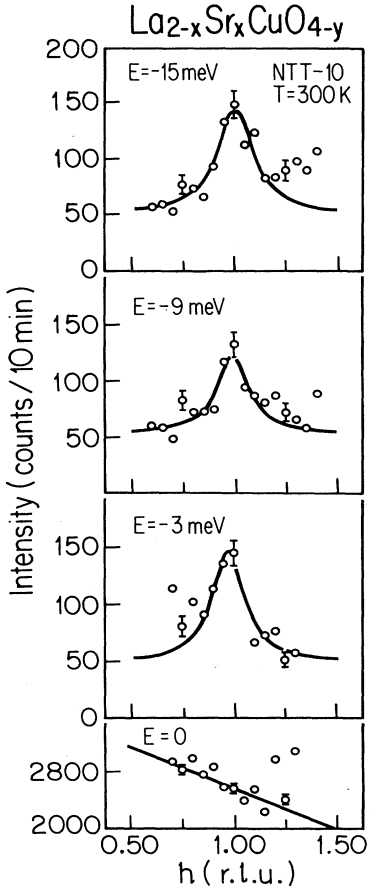

FIG. 10. Constant-E scans across the 2D magnetic rod in NTT-10. The configurations for these scans are identical to those in Fig. 6.

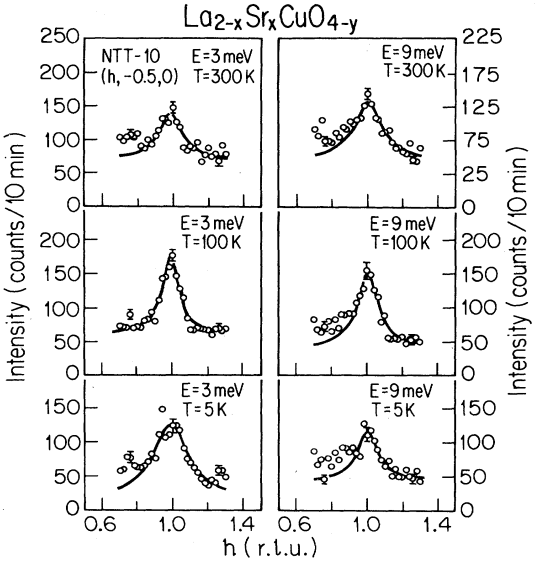

FIG. 11. Temperature dependence of the 3 and 9 meV scattering in NTT-10. The spectrometer was set in the E_f-fixed mode at 14.7 meV and the collimation was 40′-40′-40′-80′.

ing (NTT-10) and superconducting (NTT-35) $La_{2-x}Sr_xCuO_{4-y}$ is one of the salient results of this paper; presumably this difference in behavior is related to the larger hole concentration and possibly the superconductivity present in NTT-35. Hints of an incommensurate structure were observed in nonsuperconducting samples of $La_{2-x}Sr_xCuO_{4-y}$, as reported in Ref. 5. However, the transport properties and strontium concentration of these samples suggested that parts of the samples were superconducting, but that the entire sample volumes did not go into the superconducting state. More experiments will be necessary to determine conclusively whether the spin state which produces the incommensurate structure is a prerequisite for the superconductivity; however, all currently available data suggest that the incommensurate spin state is indeed a prerequisite.

In order to gain some insight into the temperature and energy dependence of the spectral distribution of the magnetic scattering, we have calculated the 1D integrated ($\int dQ$) intensity of the scattering; that is, we have found the area under the curves shown in Figs. 6–11. The results of these calculations are summarized in Figs. 12 and 13. We emphasize that a true comparison of the spectral weight can only be obtained from integrals over one Brillouin zone in Q space; however, since we do not know the complete geometry of $S(\mathbf{Q},\omega)$, the results from 1D integrations are presented here. We do not expect that this approximation will change our results qualitatively.

In Fig. 12, we show the integrated intensity at various energy transfers for NTT-10 and NTT-35 at 300 K. Corrections for the $\tan(\theta_A)/k_f^3$ factor[22] and magnetic form factor have been included in this figure, and the intensity has been normalized by the volumes of the samples. The large energy scale for the magnetic fluctuations observed in undoped and lightly doped $La_{2-x}Sr_xCuO_{4-y}$ is also present in superconducting samples; the scattering at 6 and 15 meV have comparable integrated intensities. We note, however, that only qualitative conclusions can be drawn from these data, since uncertainties in the background and the focusing effects introduce considerable errors. One may nonetheless conclude that the integrated scattering intensity is, to within a factor of 2, independent of both hole concentration and energy over the

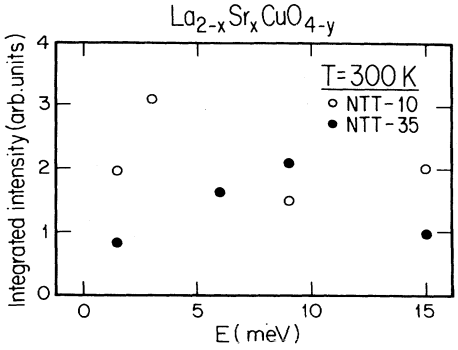

FIG. 12. Integrated ($\int dQ$) intensity vs energy transfer for NTT-10 and NTT-35 at 300 K.

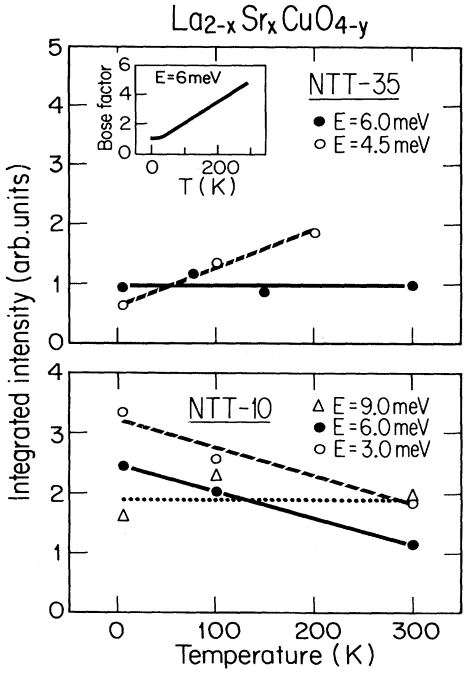

FIG. 13. Integrated ($\int dQ$) intensity vs temperature for NTT-10 and NTT-35. The data in this figure were taken at a variety of different experimental conditions; consequently the magnitude of the intensities cannot be compared at different energy transfers and between the two samples.

ranges probed here.

The temperature dependence of the integrated intensity is summarized in Fig. 13. A surprising result is that the scattering intensity is nearly temperature independent over the entire temperature range 5 K $< T <$ 300 K at 9 meV in the nonsuperconducting sample and at 6 meV in the superconducting sample. The lack of temperature dependence is very unusual, and in fact $La_{2-x}Sr_xCuO_{4-y}$ appears to be the first antiferromagnet where this behavior has been encountered. As a cross check to test this behavior, we performed scans at both +6 and −6 meV on NTT-35. As can be seen in Fig. 7, the scattering at −6 meV decreases as the temperature is lowered. This is in accord with detailed balance,[12] which states that

$$S(\mathbf{Q},-\omega)=e^{-\beta\omega}S(\mathbf{Q},\omega)\ , \tag{2}$$

where $\beta=1/k_BT$. In Fig. 7 the line through the −6 meV scattering is actually calculated from a fit to the +6 meV scattering scaled by the detailed balance factor. Thus, the measured scattering is intrinsic with little or no contamination from parasitic scattering events. We show in the inset of Fig. 13 the Bose occupation scattering factor, $1+1/(e^{(E/k_BT)}-1)$, for 6 meV excitations. For conventional phonons and magnons, the intensity of the scattering would follow the Bose factor, since the line shape is independent of temperature. The observed temperature independence provides strong evidence that the measured scattering has not originated from phonons, since the intensity of phonon scattering processes must follow the Bose statistics population factor, barring any pathologies in the temperature dependence of the phonon structure factor.

A major difference in the temperature dependence of the intensity of the superconducting and nonsuperconducting samples is that at lower-energy transfers the intensity decreases with decreasing temperature in the superconducting sample, while it increases with decreasing temperature in the nonsuperconducting sample. When contrasted with the behavior seen in the nonsuperconducting sample, the decrease in the 4.5 meV intensity with decreasing temperature observed in the superconducting sample does suggest that the scattering is moving to higher energies. One explanation for this behavior is that a gap is forming in the magnetic excitation spectrum of the superconducting sample; this behavior has been explored more thoroughly in a $T_c=33$ K sample.[21]

Unfortunately, polarized neutron scattering experiments, which could establish definitively that the inelastic signal is magnetic, as opposed to nuclear, cannot be done because the signal is too weak. Thus two other methods were used to confirm the magnetic origin of the inelastic scattering measured in NTT-35.

In the first cross check, scans across the $(1,k)$ and $(3,k)$ rod positions with the energy transfer set at 6 meV were performed; the data are shown in Fig. 14. Now if the incommensurate structure originated from phonon scattering the signal would have increased roughly as Q^2, assuming that the dynamic structure factor for the phonon scattering is approximately constant. A scan across the $(3,k)$ position would therefore have shown a double-peak structure ~9 times more intense than the equivalent scan

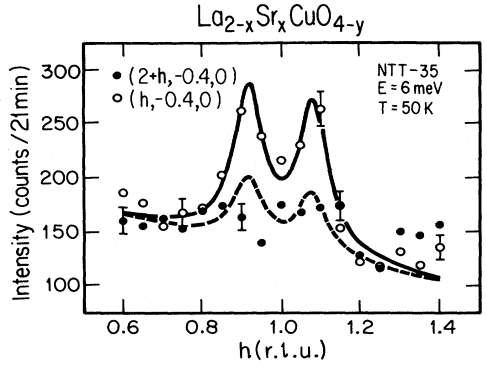

FIG. 14. Constant-E scans across the $(1,k,0)$ and $(3,k,0)$ magnetic rods. The spectrometer was set in the E_f-fixed mode at 30.5 meV and the collimation was 40′-40′-40′-80′. The dashed line is the solid line scaled by 0.40, the intensity change predicted for a magnetic signal.

at the $(1,k)$ position. On the other hand, if the scattering is magnetic in origin, due to the Cu^{+2} antiferromagnetic form factor[24] the scattering intensity would decrease by a factor of ~0.4 in going from $(1,k)$ to $(3,k)$. The dashed line in Fig. 14 is the $(1,k)$ rod data scaled by 0.40. Clearly the data are consistent only with a magnetic origin for the scattering. Moreover, this result demonstrates that virtually all of the double-peak signal is magnetic; this is information that could not easily be obtained from polarized neutron scattering experiments.

In the second crosscheck, a 6 meV scan in which the momentum transfer was scanned up the 2D Bragg rod was performed. The data are shown in Fig. 15, where it can be seen that the signal is independent of k, thus demonstrating that the scattering at this energy is entirely two dimensional. The 2D character of this scattering was actually proven indirectly in previous[10] double-axis measurements; the data presented here show this aspect of the scattering more convincingly. The 2D character of the scattering provides further evidence that the signal is magnetic, since the dynamic magnetic signal in undoped

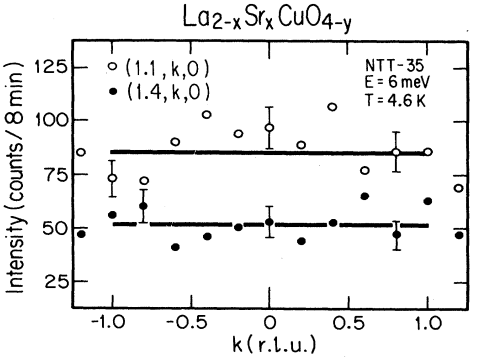

FIG. 15. Constant-E scan in which the momentum transfer was scanned along the 2D magnetic rod. The spectrometer was set in the E_f-fixed mode at 30.5 meV and the collimation was 40′-40′-40′-80′.

La_2CuO_4 has been definitively established to have a similar 2D character, while the low energy phonon modes have fully 3D dispersion relations.

VI. DISCUSSION

The results reported here put a variety of constraints on theories of the superconductivity and magnetism in $La_{2-x}Sr_xCuO_{4-y}$. Whether the short-range incommensurate spin structure that we have documented should be viewed as resulting from an incommensurate spin density wave (SDW),[25] as a frustrated state of predominately localized spins,[26] or as a spiral state arising from induced dipole interaction due to the motion of holes[27] is one of the issues which must be addressed.

In the SDW picture,[25] an incommensurate spin state occurs if the wave vector of the spin-density wave follows the Fermi wave vector with doping rather than being pinned to the lattice wave vector. An important test of this theory is that it produce the correct geometry for $S(\mathbf{Q},\omega)$. In the itinerant picture, the geometry of the 2D Fermi surface[28] is such that $S(\mathbf{Q},\omega)$ would have four rods of scattering rather than a ring of scattering.

An alternative point of view to the itinerant picture is that the Cu moments are primarily localized on Cu sites as the result of correlation effects. In a localized picture, mechanisms by which doped holes produce an incommensurate type of structure will most likely be related to either frustration[26] or hole motion.[27] Our data indicate that this incommensurability only becomes measurable in superconducting samples with relatively long localization lengths; this would seem to support the approach of Shraiman and Siggia.[27] Indeed, it is possible that the spin state associated with the incommensurability is a prerequisite for superconductivity to exist. That is, the extra kinetic energy gained by the holes when the Cu^{2+} spins go into an incommensurate state may trigger the superconductivity. We mention that localized spin approaches can produce an $S(\mathbf{Q},\omega)$ which has either four rods of scattering[27] or a ring of scattering.[29] The data presented here do not distinguish between these two possibilities; as noted previously, we will attempt to resolve this issue in future experiments.

In a recent paper,[30] the temperature-dependent part of the uniform susceptibility of $La_{2-x}Sr_xCuO_{4-y}$ was analyzed using a combination of a Pauli term and a 2D antiferromagnetic Heisenberg term with both the Cu^{2+} moment and the Cu^{2+}-Cu^{2+} exchange energy depending on hole concentration. It was suggested that both the moment and the exchange energy decreased dramatically with increasing hole concentration, with both of these quantities approaching zero at $p \sim 0.20$. This model is inconsistent with our data for at least two reasons: (i) The spin configuration in superconducting samples of $La_{2-x}Sr_xCuO_{4-y}$ is not antiferromagnetic, but rather some type of short-range incommensurate structure. (ii) The antiferromagnetic correlation length of the 2D Heisenberg model diverges as the temperature approaches zero. Our data show no evidence for such divergent behavior; indeed, the correlation length of the spin configurations which we have observed is nearly temperature independent below 300 K and is quite short.

The experiments reported here provide a picture of the energy spectrum of the spin excitations in $La_{2-x}Sr_xCuO_{4-y}$ including the following elements: (i) The integrated ($\int dQ$) scattering intensity is within a factor of 2 independent of energy transfer over the range 1.5–15 meV. (ii) The integrated ($\int dQ$) intensity of the positive energy-transfer dynamic scattering is within experimental error independent of temperature over the range $k_BT \gg \hbar\omega$ to $k_BT \ll \hbar\omega$.

Point (i) above may be explainable by the large exchange constant[2,4] ($|J| \sim 120$ meV) compounded with the fact that anharmonicity produced by quantum fluctuations creates more scattering at large energy scales. The behavior described in (ii) does not have an obvious explanation, however. The mystery in this behavior is that the intensity is temperature independent for temperatures both above and below the characteristic temperature of the magnetic excitation. It would therefore seem as if another energy scale exists in this system in addition to the thermal energy scale. We regard the lack of temperature dependence of the scattering intensity as a fundamental experimental result which any successful theory of the magnetism in this system must satisfactorily explain.

We discuss now the possible appearance of a gap in the magnetic excitation spectrum of the superconducting samples. Most recent experiments seem to favor singlet-state pairing,[31] in which case magnetic interactions can break the Cooper pairs if there is sufficient overlap between the magnetic ions and the superconducting carriers. The simplest way in which this can be prevented is if a gap appears in the spin excitation spectrum. The relevant energy scale to consider is the superconducting gap energy 2Δ. We take as the lower limit for the superconducting gap value the weak coupling Bardeen-Cooper-Schrieffer (BCS) value $2\Delta(0) = 3.5k_BT_c$; fluctuation effects,[32] anisotropy in the gap,[33] and strong-coupling effects may effectively increase this value considerably. In our $T_c = 10$ K samples the gap would then be at least $3.5k_BT_c \sim 3$ meV. The data shown in Figs. 8 and 13 do indicate that the magnetic signal at 4.5 meV in NTT-35 decreases considerably between 200 and 5 K. Moreover, Shirane *et al.*[21] have found that in a $T_c = 33$ K sample the intensity of the magnetic scattering for all energy transfers less than ~ 9 meV decreased by a factor of ~ 3 between 100 and 50 K. Thus, there is growing evidence that a gap in the magnetic excitation spectrum does in fact exist in superconducting samples of $La_{2-x}Sr_xCuO_{4-y}$; this issue is discussed more thoroughly in Ref. 21.

In conclusion, we remark that the differences we have observed in the magnetic properties of nonsuperconducting (NTT-10) and superconducting (NTT-30 and NTT-35) samples of $La_{2-x}Sr_xCuO_{4-y}$ cannot be coincidental. The magnetism and the superconductivity in $La_{2-x}Sr_xCuO_{4-y}$ are intimately related.

ACKNOWLEDGMENTS

We would like to acknowledge many helpful discussions with our colleagues at The Massachusetts Institute of Technology (MIT), Brookhaven National Laboratory, Tohoku University, and Nippon Telegraph and Telephone (NTT). We also thank Peter Gehring for his assistance with some of the measurements, and Ben Sternlieb and Yasutomo Uemura for allowing us to quote their μSR results prior to publication. This work was supported by the U.S.–Japan Cooperative Neutron Scattering Program. The work at Tohoku University was supported by a Grant-In-Aid for Scientific Research from the Japanese Ministry of Education, Science and Culture. The work at MIT was supported by the U.S. National Science Foundation under Contract Nos. DMR-85-01856 and DMR-87-19217. Research at Brookhaven National Laboratory was supported by the Division of Materials Science, the Office of Basic Energy Science of the U.S. Department of Energy, under Contract No. DE-AC02-CH00016.

---

*Also at Brookhaven National Laboratory, Upton, NY 11973-6000.

†Permanent address: Department of Materials Science, Tsukuba University, Tsukuba, Ibaraki-ken 305, Japan.

[1]D. Vaknin, S. K. Sinha, D. E. Moncton, D. C. Johnston, J. M. Newsom, C. R. Safinya, and H. E. King, Jr., Phys. Rev. Lett. **58**, 2802 (1987); K. Yamada, E. Kudo, Y. Endoh, Y. Hidaka, M. Oda, M. Suzuki, and T. Murakami, Solid State Commun. **64**, 753 (1987).

[2]G. Shirane, Y. Endoh, R. J. Birgeneau, M. A. Kastner, Y. Hidaka, M. Oda, M. Suzuki, and T. Murakami, Phys. Rev. Lett. **59**, 1613 (1987); Y. Endoh, K. Yamada, R. J. Birgeneau, D. R. Gabbe, H. P. Jenssen, M. A. Kastner, C. J. Peters, P. J. Picone, T. R. Thurston, J. M. Tranquada, G. Shirane, Y. Hidaka, M. Oda, Y. Enomoto, M. Suzuki, and T. Murakami, Phys. Rev. B **37**, 7443 (1988).

[3]Y. J. Uemura, W. J. Kossler, X. H. Yu, J. R. Kempton, H. E. Schone, D. Opie, C. E. Stronach, D. C. Johnston, M. S. Alvarez, and D. P. Goshorn, Phys. Rev. Lett. **59**, 1045 (1987).

[4]K. B. Lyons, P. A. Fleury, J. P. Remeika, A. S. Cooper, and T. J. Negran, Phys. Rev. B **37**, 2353 (1988); S. Sugai, S. Shamoto, and M. Sato, *ibid.* **38**, 6436 (1988).

[5]R. J. Birgeneau, D. R. Gabbe, H. P. Jenssen, M. A. Kastner, P. J. Picone, T. R. Thurston, G. Shirane, Y. Endoh, M. Sato, K. Yamada, Y. Hidaka, M. Oda, Y. Enomoto, M. Suzuki, and T. Murakami, Phys. Rev. B **38**, 6614 (1988).

[6]P. Gutsmiedl, G. Wolff, and K. Andres, Phys. Rev. B **36**, 4043 (1987); J. M. Tranquada, S. L. Heald, and A. R. Moodenbaugh, *ibid.* **36**, 5263 (1987).

[7]Y. Kitaoka, S. Hiramatsu, K. Ishida, T. Kohara, and K. Asayama, J. Phys. Soc. Jpn. **56**, 3024 (1987); Y. Kitaoka, K. Ishida, S. Hiramatu, and K. Asayama, *ibid.* **57**, 734 (1988).

[8]J. L. Budnick, B. Chamberland, D. P. Yang, Ch. Niedermayer, A. Golnik, E. Recknagel, M. Rossmanith, and A. Weidinger, Europhys. Lett. **5**, 651 (1988); D. R. Harshman, G. Aeppli, G. P. Espinosa, A. S. Cooper, J. P. Remeika, E. J. Ansaldo, T. M. Riseman, D. L. Williams, D. R. Noakes, B. Ellman, and T. F. Rosenbaum, Phys. Rev. B **38**, 852 (1988); Y. J. Uemura *et al.*, J. Phys. (Paris) (in press); H. Kitazawa, K. Katsumata, E. Torikai, and K. Nagamine, Solid State Commun. **67**, 1191 (1988); A. Weidinger, Ch. Niedermayer, A. Golnik, R. Simon, E. Recknagel, J. I. Budnick, B. Chamberland, and C. Baines, Phys. Rev. Lett. **62**, 102 (1989).

[9]H. Yoshizawa, S. Mitsuda, H. Kitazawa, and K. Katsumata, J. Phys. Soc. Jpn. **57**, 3686 (1988).

[10]R. J. Birgeneau, Y. Endoh, Y. Hidaka, K. Kakurai, M. A. Kastner, T. Murakami, G. Shirane, T. R. Thurston, and K. Yamada, Phys. Rev. B **39**, 2868 (1989).

[11]Y. Hidaka, Y. Enomoto, M. Suzuki, M. Oda, and T. Murakami, J. Cryst. Growth **85**, 581 (1987).

[12]W. Marshall and R. Lowde, Rep. Prog. Phys. **31**, 705 (1968).

[13]M. J. Cooper and R. Nathans, Acta Crystallogr. **23**, 357 (1967).

[14]N. W. Preyer, R. J. Birgeneau, C. Y. Chen, D. R. Gabbe, H. P. Jenssen, M. A. Kastner, P. J. Picone, and Tineke Thio, Phys. Rev. B **39**, 11 563 (1989).

[15]M. A. Kastner, R. J. Birgeneau, C. Y. Chen, Y. M. Chiang, D. R. Gabbe, H. P. Jenssen, T. Junk, C. J. Peters, P. J. Picone, Tineke Thio, T. R. Thurston, and H. L. Tuller, Phys. Rev. B **37**, 111 (1988).

[16]P. A. Lee and T. V. Ramakrishnan, Rev. Mod. Phys. **57**, 287 (1985).

[17]Y. Hidaka (private communication).

[18]Y. J. Uemura and B. Sternlieb (private communication).

[19]D. C. Johnston, S. K. Sinha, A. J. Jacobson, and J. M. Newsam, Physica C **153-155**, 572 (1988).

[20]J. B. Torrance, Y. Tokura, A. I. Nazzal, A. Bezinge, T. C. Huang, and S. S. P. Parkin, Phys. Rev. Lett. **61**, 1127 (1988).

[21]G. Shirane *et al.*, Phys. Rev. Lett. **63**, 330 (1989).

[22]N. J. Chesser and J. D. Axe, Acta Crystallogr. **23**, 357 (1973).

[23]R. A. Cowley, G. Shirane, R. J. Birgeneau, and H. J. Guggenheim, Phys. Rev. B **15**, 4292 (1977).

[24]T. Freltoft, G. Shirane, S. Mitsuda, J. P. Remeika, and A. S. Cooper, Phys. Rev. B **37**, 137 (1988).

[25]J. R. Schrieffer, X.-G. Wen, and S.-C. Zhang, Phys. Rev. Lett. **60**, 944 (1988).

[26]A. Aharony, R. J. Birgeneau, A. Coniglio, M. A. Kastner, and H. E. Stanley, Phys. Rev. Lett. **60**, 1330 (1988).

[27]B. I. Shraiman and E. D. Siggia, Phys. Rev. Lett. **61**, 467 (1988).

[28]L. F. Mattheiss, Phys. Rev. Lett. **58**, 1028 (1987).

[29]C. L. Kane (private communication).

[30]D. C. Johnston, Phys. Rev. Lett. **62**, 957 (1989).

[31]L. Krusin-Elbaum, R. L. Greene, F. Holtzberg, A. P. Malozemoff, and Y. Yeshuran, Phys. Rev. Lett. **62**, 217 (1989); D. R. Harshman, L. F. Schneemeyer, J. V. Waszczak, G. Aeppli, R. J. Cava, B. Batlogg, L. W. Rupp, E. J. Ansaldo, and D. Ll. Williams, Phys. Rev. B **39**, 851 (1989).

[32]A. Kapitulnik, M. R. Beasley, C. Castellani, and C. Di Castro, Phys. Rev. B **37**, 537 (1988).

[33]S. L. Cooper, F. Slakey, M. V. Klein, J. P. Rice, E. D. Bukowski, and D. M. Ginsberg, Phys. Rev. B **38**, 11 934 (1988).